NMR analysis of structure and assembly for Nile Blue (C. I. Basic Blue 12) and Thionine (C. I. 52000) in solution

by

David Hazafy[a], Marie Virginie-Salvia[a], Andrew Mills[a], Michael G. Hutchings[c], Maxim P. Evstigneev[b] and John A. Parkinson[a*]

[a]WestCHEM Department of Pure and Applied Chemistry, University of Strathclyde, 295 Cathedral Street, Glasgow G1 1XL, U. K.

[b]Department of Physics, Sevastopol National Technical University, Sevastopol 99053, Crimea, Ukraine.

[c]School of Chemistry, University of Manchester, Oxford Road, Manchester M13 9PL, U. K.

[*] Corresponding Author:

Dr. John A. Parkinson
WestCHEM, Department of Pure and Applied Chemistry,
University of Strathclyde,
295 Cathedral Street,
Glasgow G1 1XL, U. K.
email: john.parkinson@strath.ac.uk
Tel. : +44 141 548 2820
Fax: +44 141 548 4822

RECEIVED DATE

TITLE RUNNING HEAD: Nile Blue and Thionine solution studies

Abstract

The dyes Nile Blue (C. I. Basic Blue 12, NB) and Thionine (C. I. 52000, TH) were examined in both ionic and neutral forms in different solvents using NMR and UV-visible Spectroscopy to firmly establish the structures of the molecules and to assess the nature and extent of their aggregating characteristics. ^{1}H and ^{13}C NMR assignments and chemical shift data were used along with (for NB) nuclear Overhauser effect information enabling a structure for self-assembly to be proposed. In both cases these data were supplemented with variable temperature, dilution and diffusion-based experimental results using ^{1}H NMR spectroscopy thereby enabling the extended aggregate structures to be assessed in terms of the relative strength of self-association and the extent to which extended aggregates could form. Full and detailed solution phase NMR analysis of such dyes, especially the two studied in this context, have either not been widely reported or have not been studied to the depth presented here. The data and their interpretation form an important addition to the analysis of this class of dye compounds and provide additional insight into the effects of self-assembly on the behaviour of such molecules in various solution-phase environments.

KEY WORDS: Nile Blue, Thionine, NMR Spectroscopy, Self-Assembly, Numerical Analysis, Molecular Modelling

1. Introduction

C. I. Basic Blue 12 (Nile Blue, NB), **1**, is a classical dye which, despite being known for more than 100 years [1] remains of current interest as the basis for the development of new dyes and stains. It belongs to a class of molecules whose basic framework is that of a benzophenoxazine, a class which also includes Nile Red, a phenoxazinone, here termed Red Nile Blue (RNB) and Meldola's Blue (C. I. Basic Blue 6, C. I. 51175). These and related compounds are extensively used in scientific applications that make use of their fluorescent and solvatochromic characteristics. For RNB such applications have recently included visualization of protein conformational changes for engineered proteins containing a 4Cys motif in a live cell setting using an arsenic-modified RNB derivative [2] whereas NB has seen application as a stain for *E. coli* in flow cytometry [3], in a modified form as a chemodosimeter for Hg^{2+} in biological media [4] and has also been used to monitor processes that depend on solvent polarity [5-7], in (F)RET [8,9] and as a photosensitizer for oxygen in photodynamic therapy applications [10,11]. The property that can make these molecules attractive as stains and imaging agents is their high fluorescence quantum yield together with their solvatochromism. In polar environments, their fluorescence is reduced significantly and additionally, for molecules that would be of general use in identifying and binding to biomolecules, their aqueous solubility is generally very poor. Active research is taking place to define aqueous analogues of these benzophenoxazines and increasing success in producing these is being achieved [12]. Such molecules show higher fluorescence quantum yields than the parent molecules, a feature related to altered aggregation characteristics. As with many flat aromatic molecules, these phenoxazine-based molecules generally self-associate. Some detail

of the manner by which this occurs has been reported and it is this aggregating property that is believed to be generally responsible for quenching the fluorescence response [13, 14, 15] and which is alleviated in polar solvents. When these molecules can be functionalized for enhanced aqueous solubility, self-assembly can be disrupted which logically leads to enhanced fluorescence [16]. Whilst many of the physical properties of these dyes have been studied, little has been reported of any fine detail on the manner in which this self-association occurs. Also in the case of NB, some confusion has occurred over what the nature of the parent molecule structure is under differing solvent conditions [17,18]. For instance, it had been suggested that under alkaline conditions a neutral hydroxy adduct may form of the type shown as **2**. As part of a wider study concerned with understanding factors influencing molecular self-assembly and the investigation of the nature of the structures of several well known dye molecules, full NMR characterization of the neutral NB adduct is reported here. UV-vis spectroscopy and mass spectrometry were also used for determining whether the red, neutral form of NB had an alternative structure or not. Full NMR and related experimental studies of both the blue and red forms of NB are therefore reported, the red form of NB being shown to be the specifically deprotonated structure **3**. For comparison purposes thionine (C. I. 52000, TH), **4**, was also studied, which under alkaline conditions had previously been reported to undergo deprotonation to form **5** rather than forming a *N*-hydroxy adduct **6** [19]. NMR data had been acquired in the former study, in which differences in ^{1}H NMR chemical shifts were observed for the dye under different solution conditions. To revisit these data and draw comparison with those acquired for NB, we carried out an additional comprehensive NMR analysis of TH. Conditions previously reported [19] were used for studying both TH and NB to enable a direct comparison to be made and additional data were used in

both cases to establish parameters associated with the self-assembly of these molecules under different solvent conditions.

2. Experimental

2.1. UV-vis Spectroscopy

All UV-visible spectrophotometric experiments were recorded on a Varian Cary50 double beam spectrophotometer, using quartz (solvent samples) or plastic (aqueous samples) 1 cm cuvettes in dry solvents of the highest available purity. Typical concentration of samples was 10^{-4} M.

2.2. NMR Sample Preparation

All solvents and samples were supplied through Sigma-Aldrich. NMR samples were prepared in methanol-d_4 in the presence and absence of alkali, in DMSO-d_6 and in pyridine-d_5. C. I. Basic Blue 12 (Nile Blue, NB) and Thionine (C. I. 52000, TH) were used as supplied without further purification. Typically dye (3.0 mg) was dissolved in the solvent of choice (0.6 mL) to give a final concentration of *ca*. 5 mg per mL (i.e. 15 mM in the case of NB). To form the deprotonated species, 100 μL of 1 M tetrabutylammoniumhydroxide in methanol was added to the solution in the NMR tube and the solution was mixed well. For NB and TH, samples were also prepared in D_2O over a range of solute concentrations. For the purposes of variable temperature and concentration dependent studies it was necessary that sample pH was maintained at a stable value. Hence all D_2O solutions were prepared buffered for pH 7.4 using

phosphate at a concentration of 100 mM in all cases. Following all solution preparations, samples were admitted to Wilmad 535-PP-7 precision 5 mm Ø NMR tubes in preparation for data collection.

2.3. NMR Spectroscopy

NMR spectra were acquired at a magnetic field of 14.1 Tesla using a Bruker Avance III NMR spectrometer operating at a ^{1}H resonance frequency of 600.13 MHz and working under TopSpin version 2.0 (Bruker Biospin, Karlsruhe, Germany) on an HP XW3300 workstation running under Windows XP. Typically all NMR spectra were acquired on the prepared samples using a broadband observe probehead equipped with a z-pulsed field gradient coil [BBO-z-atm]. One-dimensional (1D) ^{13}C-{^{1}H} NMR spectra were acquired over a frequency width of 33.3 kHz (220 ppm) centred at a frequency offset equivalent to 100 ppm. Typically data from 50,000 transients were digitized into 32786 data points using an acquisition time aq = 0.5 s and a relaxation delay, d1 = 0.7 s. 1D ^{1}H NMR spectra were acquired over a frequency width of 12.3 kHz (20.55 ppm) centred at a frequency offset equivalent to 6.175 ppm into 65536 data points during an acquisition time aq = 2.66 s with a relaxation delay d1 = 2 s for each of 32 transients. Phase-sensitive two-dimensional (2D) [^{1}H, ^{13}C] HSQC NMR spectra were acquired using a sensitivity improved, gradient coherence selection pulse programme in an echo/anti-echo acquisition mode (Bruker pulse programme hsqcetgpsi2). Typically 4 transients were acquired over frequency widths of ω_2 = 6 kHz (10 ppm) and ω_1 = 25.6 kHz (170 ppm) into 2048 complex data points for each of 256 t_1 increments (aq[ω_2] = 170 ms, aq[ω_1]$_{max}$ = 5 ms) with a relaxation delay d1 = 2.0 s. Absolute value 2D [^{1}H, ^{13}C] HMBC NMR spectra were acquired without

decoupling during the acquisition time and with gradient selection and a low-pass filter (Bruker pulse programme hmbcgplpndqf). Typically 64 transients were acquired over frequency widths of ω_2 = 6 kHz (10 ppm) and ω_1 = 33.55 kHz (222 ppm) into 2048 complex data points for each of 256 t_1 increments (aq[ω_2] = 170 ms, aq[ω_1]$_{max}$ = 3.8 ms) with a relaxation delay d1 = 2.0 s. 2D [^{1}H, ^{1}H] NOESY, COSY and TOCSY NMR data were typically acquired phase sensitive a using State-TPPI mode of data acquisition over frequency widths $\omega_2 = \omega_1$ = 6 kHz (10 ppm) into 2048 complex data points with 16 transients for each of 256 t_1 increments. Mixing times, τ_m, were as follows: for TOCSY data sets τ_m = 70 ms; for NOESY data sets τ_m = 200 ms, 270 ms and 1000 ms. For NOESY and TOCSY data sets acquired on samples solubilized in pyridine-d_5, a WET solvent suppression scheme [20] was used with ^{13}C decoupling during the solvent signal selective pulses to cleanly suppress the residual pyridine solvent signals without undue disruption of the NMR signals associated with the solute. Diffusion measurements were carried out using a bipolar gradient pulse program (Bruker pulse program ledbpgppr2s) in which presaturation was used to suppress the residual solvent signal during the recycle delay. Typically 32 gradient increments were used by which the gradient strength was varied linearly in the range 2% to 95% of full gradient strength (54 G/cm with a rectangular gradient) using a sine-shaped gradient. Typically the gradient pulse duration was set to 1 ms and the diffusion period to 200 ms. With increasingly dilute samples, the number of transients was increased accordingly in order to allow for diffusion coefficients to be evaluated with a reasonable fit of the experimental data to theory (i.e. number of transients (NS) per FID varied in the range NS = 32 to NS = 256 for sample concentrations in the range 5 mM to 0.2 mM). The robustness of the approach used for diffusion measurements against the effects of convection were assessed by use of a convection

compensating pulse program. Within experimental error no differences were found in the results observed using the convection compensated approach compared with the non-compensated approach, thereby validating the method adopted for this study. Diffusion data were processed under TopSpin (version 2.0, Bruker Biospin) using the T1/T2 analysis module in order to fit the data to the standard expression of diffusion coefficient as a function of gradient strength.

2.4. Mass spectrometry

MS spectra for both forms of NB and TH were recorded using an ESI-MS (ThermoFinnigan LCQ DUO MS) instrument using the direct injection port. An LDI-MS (Shimadzu, AXIM-CFR) was also used to record MS spectra of NB and TH. MS spectra on commercial NB and TH samples were also recorded for comparison purposes.

2.5. Molecular Modelling

Structural models used to aid visualization of the non-covalent self-assembly of molecules used in these studies were built within Sybyl (Version 6.3, Tripos Inc.,) running on a Silicon Graphics Extreme workstation operating under IRIX version 5.2. Crude structures were energy minimized using 500 steps of a conjugate gradient energy minimization molecular mechanics routine. Charges were applied using a Gasteiger-Huckel routine. Pairs of minimized structures were manually manipulated in order to match inter-molecular NOEs. Key inter-proton restraints were applied to dimers using a range restraint of 2.5-3.5 Å with a force constant of 10 kcal mol^{-1} $Å^2$.

1000 steps of conjugate gradient energy minimization were applied to allow the restraints to guide the orientation of molecules with respect to one another and to reduce instances of bad contacts.

2.6. Numerical Analysis

The experimental NMR dilution and variable temperature data were analysed in terms of an indefinite non-cooperative model of association [23], which assumes sequential addition of the monomer X to an aggregate X_{i-1} containing i-1 molecules, with equilibrium self-association constant K. The key relations are given by the dependence of the experimentally observed chemical shift, δ, on the concentration of the dye, x_0 [23] in which

$$\delta = \delta_m + (\delta_d - \delta_m) \cdot \frac{2Kx_0 + 1 - \sqrt{4Kx_0 + 1}}{Kx_0}, \qquad (1)$$

where δ_m and δ_d are the chemical shifts in monomer and dimer forms (or at the ends of an aggregate) of the dye in solution, respectively. Minimisation of a discrepancy function between the experimental $\delta(x_0)$ and theoretical (eqn.(1)) chemical shifts results in the calculation of optimal values of the variable parameters (K, δ_m, δ_d). The thermodynamical parameters, enthalpy (ΔH) and entropy (ΔS), for the self-association reaction were calculated from the temperature dependencies of ^{1}H chemical shifts replacing the K value in equation (1) by the corresponding relation $K(T)$ according to the van't Hoff's formalism [23]:

$$K(T) = exp(\Delta S/R - \Delta H/RT) \qquad (2)$$

In order to increase the quality of fit of the calculated thermodynamical parameters in this work, two sets of variable temperature data were used within the numerical analysis namely at high (x_0 = 2 mM) and low (x_0 = 0.2 mM) concentrations of the dye.

3. Results and Discussion

3.1: Nile Blue (NB)

Figure 1a shows the UV-vis absorption spectra of NB recorded under different solution conditions, the results of which were very similar to those reported by Pal and coworkers [17] with a similar hypsochromic shift on formation of the neutral dye. Using this as confirmatory evidence that the species formed in our hands on treatment of a NB solution with 0.1 M NaOH and subsequent separation using toluene was the same as that observed by Pal and coworkers, we progressed to analyse the NMR data acquired for the two forms of the dye under various solvent conditions, namely in water and in methanol or pyridine. **Figure 1b** shows (in the screw capped vial) the result of the addition of alkali to a concentrated aqueous solution of NB with the added presence of toluene. After shaking and allowing for a settling period, the lower (aqueous) layer was seen to contain the blue form of NB whilst the upper layer clearly contained the orange-red form of the dye, namely red Nile Blue (RNB). The NMR sample in **Figure 1b** was of RNB in pyridine-d_5. Both the ionic (blue) and neutral (red) forms of NB were also studied in methanol-d_4 by NMR.

Figure 1 Here

Structures were proposed by comparison of the chemical shift assignments and nuclear Overhauser effect (NOE) responses from the NMR data. As a starting point the initial NMR analysis of NB was carried out on a sample solubilized in DMSO-d_6. This allowed resonances associated with labile protons to be observed. Assigned 1D ^{1}H and ^{13}C-{^{1}H} NMR spectra for NB and RNB are presented in **Figures 2** and **3**. The ^{1}H NMR data showed a single molecule impurity up to a level of *ca*. 10% typically associated with a molecule of very similar structure corresponding to a substitution product formed in the material synthesis. The presence of this impurity was distinct from and much lower in concentration than the molecule of interest and was therefore deemed not to influence the NMR data interpretation that would follow. The numbering scheme for NB and the related RNB are presented with **1**.

Figure 2 and Figure 3 Here

The NMR data were interpreted as follows. Proton NMR resonances associated with ring **A** of **1** gave rise to a classical pattern of two double doublets (signals at δ^{1}H = 8.45 and 8.76 ppm representing H12 or H15) and two double double doublets (signals at δ^{1}H = 7.86 and 7.97 ppm representing H13 or H14) with larger signal splitting arising from $^{3}J_{\text{ortho}}$ couplings among aromatic resonances from protons adjacent to one another in the aromatic spin system. A singlet (δ^{1}H = 6.86 ppm) was assigned to H9. A classical ABX spin system was observed for proton resonances associated with ring **D**. 2D [^{1}H, ^{1}H] COSY NMR data (**Figure 4**) were consistent with the coupling networks in both cases. In order to correctly assign the NMR resonances associated with protons in ring **A** relative to ring **B**, 2D [^{1}H, ^{1}H] NOESY NMR data were assessed for relevant intra-molecular proximity of protons to one another. The

200 ms 2D [^{1}H, ^{1}H] NOESY NMR data (**Figure 5**) acquired for NB in DMSO-d_6 showed several notable features, one of which was a pair of broad singlet resonances at δ^1H = 9.88 and 9.80 ppm which characteristically corresponded to signals associated with NH_2 attached to ring **B** of the NB structure. Several features of these resonances are worthy of comment.

Figure 4 and Figure 5 Here

Firstly the resonances were broad but resolved and as indicated by the NOE data, were clearly the subject of a chemical exchange process that was slow on the NMR timescale. The amine protons were thus exchanging by slow rotation about the N-C^{10} bond of ring **B**. Assignment of NOEs associated with the amine protons enabled clear identification to be made of resonances from protons attached to ring **A** of NB. Thus the double doublet resonance at δ^1H = 8.76 ppm was assigned to H15 by virtue of a large ^3J scalar coupling and 2D [^{1}H, ^{1}H] COSY NMR correlation to a ddd signal at δ^1H = 7.97 ppm (H14) combined with the absence of a NOE cross-peak to the amine proton resonance at 9.88 ppm in the 2D [^{1}H, ^{1}H] NOESY NMR data. The ddd H14 was coupled to the triplet at δ^1H = 7.86 ppm which was assigned to H13 and this in turn showed coupling to the double doublet at δ^1H = 8.45 ppm. This resonance also showed a NOE cross-peak to the amine protons and was thus assigned to H12. A NOE correlation between the amine proton resonances and a sharp singlet at δ^1H = 6.86 ppm enabled the latter to be assigned firmly to H9. NOE correlations between the resonances associated with the ethyl CH_2 protons and the remaining aromatic resonances also supported their subsequent assignment. All proton assignment and

related coupling information for NB dissolved in two different solvents are summarized in **Table 1**.

Table 1 Here

Data analysis for a DMSO-d_6 solution was necessary for NB in order to correctly assign the ring **A** proton resonances, only achievable by recourse to observable NOE correlations to the exchangeable amine protons, for which resonances were not visible in the data acquired on NB dissolved in methanol-d_4. The high chemical shift noted for the amine proton resonances was indicative of likely electrostatic interactions with neighbouring molecules and was further investigated by analysis of the NOE data as part of the self-association study of these molecules (*vide infra*).

Since RNB was insoluble in DMSO-d_6 due to the neutral nature of the molecule, it was necessary to make signal assignments for both NB and RNB in methanol-d_4 for suitable comparisons to be made. The ^{13}C NMR data assignment for NB (**Table 1**) was made by reference to 2D [^{1}H, ^{13}C] HSQC and HMBC NMR data sets (**Figure 6a**). Full analysis of the data was achieved enabling all ^{13}C NMR resonances from the carbon skeleton framework to be assigned.

Figure 6 Here

3.2. Red Nile Blue (RNB)

The NMR data for the red form of NB (RNB) were assigned under suitable conditions with respect to data acquired for NB. In order to firmly establish the structure of RNB it was necessary to find conditions under which observation of exchangeable proton resonances could be made. DMSO-d_6 was unsuitable as a solvent and methanol-d_3 (CD_3OH) was excluded on the expectation of fast exchange existing for labile protons of RNB with the solvent. As an alternative, pyridine-d_5 was found to be suitable into which RNB could be extracted. Moreover, the UV-vis responses for RNB in pyridine-d_5 and in aqueous NaOH were very similar in profile and showed virtually identical λ_{max} values. This indicated the strong likelihood of the same species being present in both solutions. The aromatic region of the 1D ^{1}H NMR spectrum of RNB in pyridine-d_5 (**Figure 7a**) showed a singlet resonance at δ^1H = 10.53 ppm which integrated to one proton equivalent. 2D [^{1}H, ^{1}H] NOESY NMR data acquired at mixing times of 270 ms and 1000 ms (**Figure 7b**) showed this signal to correlate most strongly with a singlet resonance at δ^1H = 6.44 ppm which was assigned to H9 on ring **B** of RNB. This was only consistent with a structure in which the amine of NB had been mono-deprotonated, with the remaining proton showing an orientation preference as shown for **3**. At the longer mixing time of 1000 ms, a much smaller NOE was also observed between the N<u>H</u> signal at δ^1H = 10.53 ppm and a signal at δ^1H = 8.8 ppm, assigned to H12 of RNB, thus indicating either a smaller preference for orientation of the N<u>H</u> in closer proximity to H12 or an effect arising from spin-diffusion.

Figure 7 Here

Assignment of all other non-exchangeable proton signals in the pyridine-d_5 solution mirrored those recorded for RNB in methanol-d_4 thus indicating structural similarity under both sets of solution phase conditions (**Table 2**).

Table 2 Here

Comparison of ^{1}H and ^{13}C NMR chemical shift data (**Table 3** and **Figure 6**) acquired for NB and RNB in methanol-d_4 solutions were consistent with such a structural change. Thus significant ^{1}H chemical shift changes ($|\Delta\delta| > 0.5$ ppm) occurred for responses as follows: H3 and H5 in close proximity to the diethylamino group (the subject of a significant electronic change in the transition from NB, **1**, to RNB, **3**) and H9 in close proximity to the amine associated with ring **B**. The most significant changes in ^{13}C chemical shifts ($|\Delta\delta| > 7.0$ ppm) occurred for C9, C10 and C11 which would be expected for a significant change in chemical and electronic structure resulting from a change occurring at the amine nitrogen attached to position 10 on ring **B**. Although smaller changes in ^{13}C chemical shifts were observed for C17 and C1 adjacent to the phenoxazine nitrogen of ring **C**, proposed as the site for *N*-hydroxy adduct formation according to Basu *et al.* [17], these changes in ^{13}C chemical shift could be explained in terms of what might be expected electronically from the conversion of **1** to **3**.

Table 3 Here

Consistent with these findings were the ESI-MS data which showed *m*/z 318 for both NB and RNB (data not shown). This is understandable since the normally

"deprotonated" RNB would be protonated (i.e. charged) when formed in the electrospray equipment for which the detected mass would be M+H = *m/z* 318, the same as NB. The latter is charged already thereby maintaining its original mass of *m/z* 318 under electrospray conditions. Our MS analysis did not produce any evidence to show a mass of *m/z* 335 as reported by others [17]. This evidence together with all of the supporting experimental evidence described here points to deprotonation at the amine of **1** to form **3** rather than hydroxylation at the phenoxazine nitrogen under basic conditions.

3.3. Self-Association

3.3.1. Thionine, TH

In an extension to this investigation, it was considered prudent to examine our findings for RNB with reference to reports of a deprotonation mechanism for thionine [19], (TH, **4**), and thus support the assertion that RNB forms from NB through the same deprotonation mechanism. This also provided an opportunity to compare and contrast the nature of the self-association characteristics of NB and TH with one another under similar conditions and to assess the differences in the assembly behaviour for TH under different solution conditions. Our initial focus on TH, **4** was in an attempt to observe amine resonances in suitable solvents, but this proved unsuccessful. Neither were two separate spin-systems observed for the aromatic protons of TH, **4**, a resonance hybrid of two forms being representative of the structure. However, measurements additional to those made previously [19], which extended to investigating additional elements of the solution behaviour of TH, were made for both the charged and neutral forms of the molecule. The 1D ^{1}H NMR

spectrum of TH, **4** was acquired in D_2O giving rise, for a 2 mM solution at 298 K, to three NMR signals at δ^1H = 7.65 ppm (d), 7.09 ppm (dd) and 6.89 ppm relative to the methyl singlet resonance of tetramethylammonium chloride (TMA) at 3.178 ppm. The 1D ^1H NMR spectrum of the neutral form of TH (expected to be **5**) in methanol-d_4, formed through the addition of NaOD, also gave rise to three NMR signals, namely at δ^1H = 7.23 ppm (d), 6.76 ppm (dd) and 6.59 ppm relative to the residual methanol solvent resonance at 3.30 ppm. Aggregation properties of the two forms of the molecule were assessed by means of variable temperature, dilution and diffusion NMR studies and these were also carried out for NB under neutral aqueous conditions, the preferred environment for biological investigations. The contrasting variable temperature responses for the two forms of TH, **4** and **5**, in their respective solvents (**Figure 8**) showed that lowering the dye concentration or increasing the temperature in D_2O solution resulted in a large apparent downfield chemical shift change.

Figure 8 Here

Such behaviour is commonly attributed to sandwich-type self-association characterised by strong shielding of aromatic protons due to ring-current effects from neighbouring molecules [21]. Such self-association was concluded for methylene blue using spectrophotometric data, which was interpreted in terms of sandwich dimer assembly occurring in a manner that resulted in maximum separation of the charge-carrying dimethylamino groups of each molecule [22]. Numerical analysis of NMR chemical shift data confirmed this type of assembly for TH, **4** (**Table 4**), quantitatively resulting in the apparent shielding ($\delta_m > \delta_d$) of all of the non-

exchangeable aromatic protons in the assembly. Deeply negative values were also calculated for the thermodynamic parameters ΔH_{agg} and ΔS_{agg} for TH, **4**, a characteristic also recognised as a feature of sandwich-type aggregation in aqueous solution [23]. The magnitudes of the equilibrium self-association constant, K_{agg}, and the thermodynamic parameters (**Table 4**) exhibit typical values for three-ring aromatic molecules studied by NMR under similar solution conditions and using the same numerical approach [23].

Table 4 Here

Diffusion coefficients measured for TH, **4**, in D_2O also showed the effect of a change in the aggregation state of the molecule with concentration by evaluation at two different concentrations: for TH at a concentration of 5 mM in D_2O, $D = 3.94 \times 10^{-10}$ m^2 s^{-1} compared with $D = 5.73 \times 10^{-10}$ m^2 s^{-1} for TH at a concentration of 0.2 mM.

In contrast to the study of TH, **4**, in D_2O, the experimental dilution and variable temperature curves for the neutral form of TH, **5**, in methanol (**Figure 8c** and **8d**), exhibited relatively negligible dependence of chemical shift on concentration and temperature, although at low concentrations downfield shifts were observed but the effects were much less pronounced compared with findings for the study in D_2O. Since these changes in proton chemical shifts were very small, the numerical analysis for the self-association of the neutral form of TH in methanol, **5**, was found to be unreliable. Nevertheless, the qualitative observations were in agreement with a sandwich-type self-assembly of **5** in methanol with much lower self-association constant than that for TH under aqueous solution conditions. It was expected that little if any change would be found in the self-diffusion coefficient of **5** in methanol upon

dilution. However, significant changes were observed: for neutral TH, **5**, at 5 mM, $D = 8.45 \times 10^{-10}$ m^2 s^{-1}, at 2 mM, $D = 1.39 \times 10^{-9}$ m^2 s^{-1} and at 0.2 mM, $D = 2.00 \times 10^{-9}$ m^2 s^{-1}. By comparing these results and conditions with those of the self-diffusion study of TH, **4**, in D_2O (see above), it may be concluded that in the concentration range used (5 mM to 0.2 mM) the changes of D in methanol were 1.63 times greater than the case for D_2O, opposing initial expectations. However, this result can be understood in terms of the considerably different hydrophobic properties of aqueous and methanol solvents with respect to the aggregation process. In D_2O, due to hydrophobic interactions, the effective removal of water molecules from the volume between the stacked dye molecules results in less than a factor of two increase in the number of solvent molecules associated with a dimer. In less polar methanol the situation is different: the hydrophobic interactions are negligible which leads to small, if any, removal of the solvent outside the dimer. Taken together, the data can be interpreted such that the number of solvent molecules associated with dimers in D_2O is much smaller than that in methanol, which can qualitatively address the inter-relation of the diffusion coefficients in these solvents.

3.3.2. Nile Blue, NB

For comparison it was possible to collect a similar series of variable temperature, concentration dependent and diffusion-related NMR data for NB under neutral aqueous conditions and these were considered in view of a model which was deduced for the possible structure of the assembly units of extended aggregates of NB in solution. This was considered for the DMSO-d_6 solution of NB, 2D [^{1}H, ^{1}H] NOESY NMR data (**Figure 5**) for which had revealed several inter-molecular NOEs,

present through NB self-association. Evidence for this arose also from the negative sign of the NOE response, an effect more typical of large molecules for which the product of the Larmor precession frequency and molecular correlation time, $\omega\tau_c >> 1$. The most prominent intermolecular NOEs were identified between proton pairs H15-H2 and H5-H9 (**Figure 5**), with several weaker responses occurring at longer mixing times (e.g. for H15-H5 and H12-H9) arising through spin-diffusion effects. The main responses were mapped onto a crude model of a self-assembly dimer structure for NB (**Figure 9**) in which one molecule was arranged relative to the other through 180° rotation along an axis between the phenoxazine N and O atoms of ring **C**.

Figure 9 Here

This arrangement of adjacent molecules results in separation of the positively charged diethylamino groups from one another and engenders a proximal relationship of the protons responsible for the largest intermolecular NOEs. On the basis of this model, an explanation for the high chemical shift values of the amine protons was revealed in terms of the electrostatic association of the N<u>H</u> of one molecule with the positively charged diethylamino group of an adjacent molecule, structurally satisfying both the high chemical shift observed for the amine proton resonances together with the creation of two magnetically distinct types of amine proton as observed from the ^{1}H NMR data of NB in DMSO-d_6.

The self-association characteristics of NB were also studied in water by monitoring the diffusion characteristics and the concentration and variable temperature dependence of proton chemical shifts. Chemical shifts were tracked and measured relative to TMA at 3.184 ppm for as many aromatic resonances as possible.

As shown (**Figure 10**) the general trend was towards an increase in chemical shift with decreasing concentration and increasing temperature. For the evolution of chemical shift with concentration the data were significant as shown for example by the behaviour of the resonance assigned to H15 where $\Delta\delta_{0.05\text{-}10mM}$ = 1.436 ppm, which is bigger than for any resonance associated with TH in D_2O (maximum $\Delta\delta_{0.05\text{-}10mM}$ = 0.559 ppm for H1).

Figure 10 Here

These data were suitable for numerical analysis to be carried out in order to establish K_{agg}, ΔH_{agg} and ΔS_{agg} for which the results are summarized (**Table 5**) and provide mean values of K_{agg}=5600 ± 1100 M^{-1}, ΔH_{agg}= -(31 ± 2) kJ.mol^{-1} and ΔS_{agg}= -(34 ± 7) J.mol^{-1}.K^{-1}. As with TH, **4**, diffusion coefficients were evaluated for NB under neutral aqueous conditions at concentrations of 5 mM and 0.2 mM for which the values $D = 1.67 \times 10^{-10}$ m^2 s^{-1} and $D = 3.99 \times 10^{-10}$ m^2 s^{-1} were obtained respectively (see **Table 6** for a summary of all diffusion coefficients).

Table 5 Here

Table 6 Here

3.3.3 Comparison of self-assembly characteristics for NB and TH in aqueous solution

From the association parameters and self-diffusion coefficients determined for both TH and NB, several points are worth noting. Firstly K_{agg} for TH, **4**, in aqueous solution is an order of magnitude smaller than for NB, **1**, under the same conditions.

Also, the self-diffusion coefficients for TH are larger than for NB at the same concentrations. Changes in self-diffusion coefficient with concentration were evaluated as $\Delta D_{TH} = 1.79 \times 10^{-10}$ m^2 s^{-1} compared with $\Delta D_{NB} = 2.32 \times 10^{-10}$ m^2 s^{-1} where $\Delta D = (D_{0.2\ mM} - D_{5\ mM})$ i.e. the change in diffusion coefficient for NB is larger than for TH under the same aqueous conditions. Together these may be interpreted by considering the aggregation state of the molecules in solution, which in turn reflects the self-quenching of the fluorescence properties of these molecules. The larger K_{agg} for NB is a feature associated with four fused aromatic rings in NB compared with three in TH, thereby providing greater opportunity for hydrophobic, van der Waals and π-π stacking interactions to occur for NB than for TH. This is mirrored in the apparent diffusion properties of the molecules: where association is stronger, the apparent diffusion coefficient is smaller underlining the fact that the aggregates have longer lifetimes compared with molecules that associate less strongly (smaller K_{agg} and larger D values). It would be of value to be able to more readily quantify the relationship between K_{agg} and D thereby allowing greater insight into the form of the extended aggregate, which would be useful in designing molecules based on those studied here either with a greater propensity for aggregation (in the case of nanostructure formation) or with a lower propensity to aggregate (in the case of enhancing the fluorescence quantum yield by disfavouring aggregation). Modelling has been attempted previously for the dye Hoechst 33258 in order to fit the measured diffusion coefficient as a function of concentration [24]. This has been in an attempt to assist with understanding shape and size of aggregating molecular assemblies. A similar approach was attempted with NB and TH as part of this study, but it was clear that the model itself is inadequate for accurately describing the assemblies formed by NB and TH in solution. We are pursuing this in more detail as part of a related

program of research and will report our findings in due course. Nevertheless, the value of combining an understanding of the self-diffusion characteristics with the self-association parameters of an aromatic molecule when considering the development of new water soluble dyes for biological application is of value provided a suitable model can be achieved. By understanding the nature of the aggregate structure and dynamics in detail as in this instance for NB, it would be plausible to more accurately design dye systems that retained fluorescence characteristics but that were prevented from auto-quenching of the fluorescence response by self-aggregation.

4. Conclusions

A comprehensive solution phase NMR study, supplemented with UV-vis spectroscopy and mass spectrometry, has been carried out on the dyes Nile Blue (C. I. Basic Blue 12, NB) and Thionine (C. I. 52000, TH) in order to confirm the structures of each molecule in both charged and neutral forms. The study was also used to examine the manner in which NB self-associates and to evaluate self-diffusion and assembly parameters with a view to relating these to the nature and behaviour of aggregate formation. It is clear from these findings that the neutral form of each molecule is achieved through mono-deprotonation of an attached amine group. For NB in particular, this was confirmed by integration of the ^{1}H NMR data of the neutral adduct and by preparing a full assignment of the resulting ^{1}H and ^{13}C NMR data. Chemical shift changes in both ^{1}H and ^{13}C NMR spectra for NB between the charged and neutral forms of the molecule reflected the structural changes thereby providing supporting evidence for the mono-deprotonated adduct. Both UV-vis and MS data

conformed to this assertion. NOE data allowed a basic model to be created for the self-assembly element of NB aggregates in which maximum separation between charges is achieved by forming dimer assemblies in a 'head-to-tail' fashion. Self-association parameters and diffusion characteristics were evaluated under various conditions to allow an appreciation to be had of the influence of structure on aggregation characteristics for these molecules and to provide information that may be of assistance in the design of water-soluble analogues of these molecules that will display less pronounced aggregation whilst retaining strong fluorescence characteristics. While existing models relating concentration and diffusion coefficient proved of no value in this instance, it is clear that significant future value will be achieved by establishing a model suitable for assessing the aggregating characteristics of such molecules on the basis of diffusion measurements, a work that is currently in progress within our laboratory.

References

[1] Möhlau R, Uhlmann K. Zur Kenntniss der Chinazin- und Oxazinfarbstoffe. Justus Liebigs Annalen der Chemie 1896; 289: 90-130.

[2] Nakanishi J, Nakajima T, Sato M, Ozawa T, Tohda K, Umezawa Y. Imaging of Conformational Changes of Proteins with a New Environment-Sensitive Fluorescent Probe Designed for Site-Specific Labeling of Recombinant Proteins in Live Cells. Analytical Chemistry 2001; 73: 2920-2928.

[3] Betscheider D, Jose J. Nile blue A for staining Escherichia coli in flow cytometer experiments. Analytical Biochemistry 2009; 384: 194-196.

[4] Lee MH, Lee SW, Kim SH, Kang C. Nanomolar Hg(II) Detection Using Nile Blue Chemodosimeter in Biological Media. Organic Letters 2009; 11: 2101-2104.

[5] Lee SH, Suh JK, Li M. Determination of Bovine Serum Albumin by Its Enhancement Effect of Nile Blue Fluorescence. Bulletin of the Korean Chemical Society 2003; 24: 45-48.

[6] Das K, Jain B, Patel HS. Nile Blue in Triton-X 100/benzene–hexane reverse micelles: a fluorescence spectroscopic study. Spectrochimica Acta Part A 2004; 60: 2059-2064.

[7] Krihak M, Murtagh MT, Shahriari MR. A Spectroscopic Study of the Effects of Various Solvents and Sol-Gel Hosts on the Chemical and Photochemical Properties of Thionin and Nile Blue A. Journal of Sol-Gel Science and Technology 1997; 10: 153-163.

[8] Maliwal BP, Kusba J, Lakowicz JR. Fluorescence energy transfer in one dimension: Frequency-domain fluorescence study of DNA-fluorophore complexes. Biopolymers 1995; 35: 245-255.

[9] Lakowicz JR, Piszczek G, Kang JS. On the Possibility of Long-Wavelength Long-Lifetime High-Quantum-Yield Luminophores. Analytical Biochemistry 2001; 288: 62-75.

[10] Lin CW, Shulok JR, Wong YK, Schambacher CF, Cincotta L, Foley JW. Photosensitization, Uptake, and Retention of Phenoxazine Nile Blue Derivatives in Human Bladder Carcinoma Cells. Cancer Research 1991; 51: 1109-1116.

[11] Lin CW, Shulok JR. Enhancement of Nile Blue Derivative-Induced Photocytotoxicity by Nigericin and Low Cytoplasmic pH. Photochemistry and Photobiology 1994; 60: 143-146.

[12] Jose J, Burgess K. Benzophenoxazine-based fluorescent dyes for labeling biomolecules. Tetrahedron 2006; 62: 11021-11037.

[13] Sautter A, Thalacker C, Heise B, Würthner F. Hydrogen bond-directed aggregation of diazadibenzoperylene dyes in low-polarity solvents and the solid state. Proceedings of the National Academy of Sciences USA 2002; 99: 4993-4996.

[14] Bujdák J, Nobuo I. Optical properties of molecular aggregates of oxazine dyes in dpespersions of clay minerals. Colloid Polymer Science 2009; 287: 157-165.

[15] Niu SL, Ulrich G, Ziessel R, Kiss A, Renad P-Y, Romieu A. Water-soluble BODIPY derivatives. Organic Letters 2009 ; 11 : 2049-2052.

[16] Pal MK. Effects of differently hydrophobic solvents on the aggregation of cationic dyes as measured by quenching of fluorescence and/or metachromasia of the dyes. Histochimie 1965; 5: 24-31.

[17] Basu S, Panigrahi S, Praharaj S, Ghosh SK, Pande S, Jana S, Pal A, Pal T. Solvent Effect on the Electronic Spectra of Azine Dyes under Alkaline Condition. Journal of Physical Chemistry A 2007; 111: 578-583.

[18] Plater MJ. A degradation product of methylene blue. ARKIVOC 2003, 37-42.

[19] Nicotra VE, Mora MF, Iglesias RA, Baruzzi AM. Spectroscopic characterization of thionine species in different media. Dyes and Pigments 2008; 76: 315-318.

[20] Smallcombe SH, Patt SL, Keifer PA. WET Solvent Suppression and Its Applications to LC NMR and High Resolution NMR Spectroscopy. Journal of Magnetic Resonance Series A 1995; 117: 295-303.

[21] Martin RB. Comparisons of indefinite self-association models. Chemical Reviews 1996; 96: 3043-3064.

[22] Patil K, Pawar R, Talap P. Self-aggregation of Methylene Blue in aqueous medium and aqueous solutions of Bu_4NBr and urea. Physical Chemistry Chemical Physics 2000; 2: 4313-4317.

[23] Davies DB, Djimant LN, Veselkov AN. ^1H NMR investigation of self-association of aromatic drug molecules in aqueous solution. Journal of the Chemical Society Faraday Transactions 1996; 92: 383-390.

[24] Buurma NJ, Haq I. Calorimetric and Spectroscopic Studies of Hoechst 33258: Self-association and Binding to Non-cognate DNA. Journal of Molecular Biology 2008; 381: 607-621.

Structures

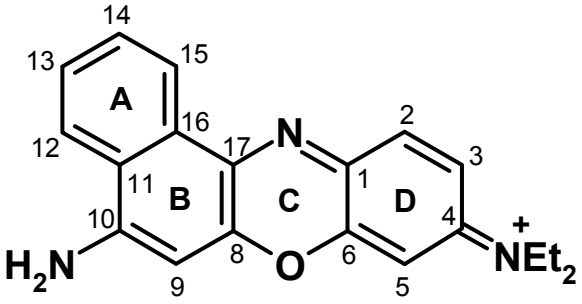

1

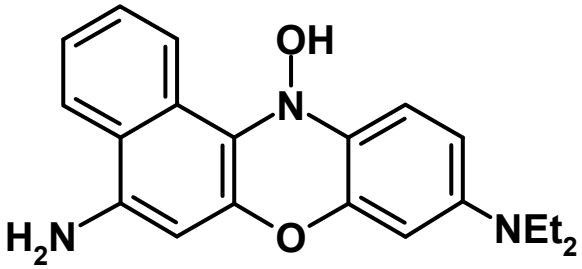

2

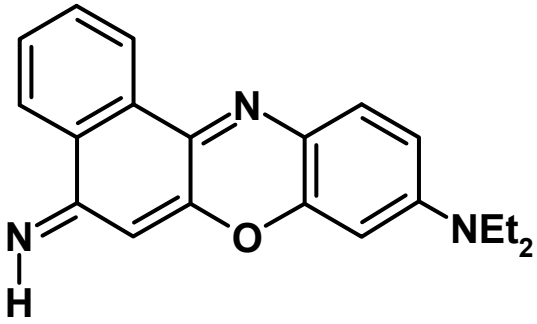

3

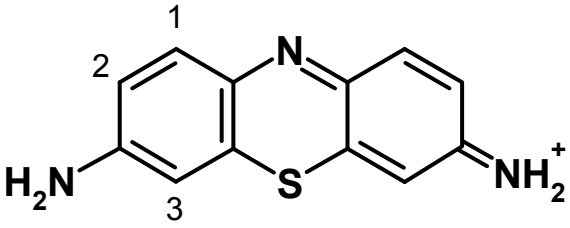

4

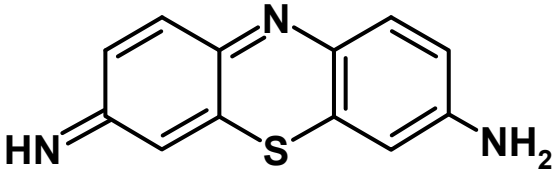

5

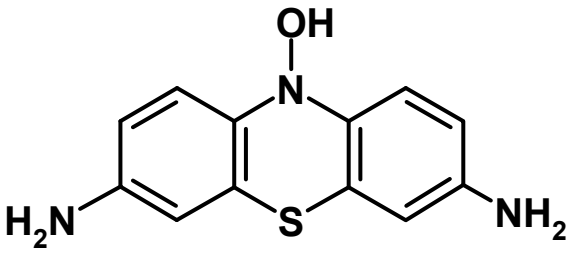

6

Table 1.

^{1}H and ^{13}C chemical shift data for NB dissolved in methanol-d_4 and DMSO-d_6.

Position	$\delta^{1}H$ (ppm)†	Multiplicity	$^{2}J_{HH}$, $^{3}J_{HH}$, $^{4}J_{HH}$	Proton Equivalents	$\delta^{13}C$ (ppm)
1	-	-	-	-	155.84
2	7.81 (7.81)	d	9.6	1	134.35
3	7.24 (7.23)	dd	9.6, 2.7	1	116.61
4	-	-	-	-	131.51
5	6.87 (6.98)	d	3	1	97.16
6	-	-	-	-	149.77
7 (O)	-	-	-	-	-
8	-	-	-	-	153.18
9	6.82 (6.86)	s	-	1	97.82
10	-	-	-	-	135.22
11	-	-	-	-	124.25
12	8.27 (8.45)	dd	8.4, 1.2	1	125.77
13	7.80 (7.86)	ddd	8.4, 7.1, 1.2	1	130.99
14	7.92 (7.97)	ddd	8.4, 7.1, 1.2	1	133.69
15	8.85 (8.76)	dd	8.4, 1.2	1	124.86
16	-	-	-	-	133.43
17	-	-	-	-	163.08
18 (N)	-	-	-	-	-
19 (N)	-	-	-	-	-
20a/b	3.69 (3.65)	q	7.2	2	47.16
21a/b	1.34 (1.22)	t	7.2	3	13.07
22 (N) a*	*(9.88)*	br s	-	1	-
22 (N) b*	*(9.80)*	br s	-	1	-

† Data from samples dissolved in DMSO-d_6 are shown bracketed.

Table 2.

^{1}H and ^{13}C chemical shift data for RNB dissolved in methanol-d_4 and pyridine-d_5.

Position	$\delta^{1}H$ (ppm)†	Appearance	$^{2}J_{HH}$, $^{3}J_{HH}$, $^{4}J_{HH}$	Proton Equivalents	$\delta^{13}C$ (ppm)
1	-	-	-	-	151.79
2	7.36 (7.81)	d	9	1	131.52
3	6.57 (6.57)	dd	9.0, 2.4	1	110.05
4	-	-	-	-	125.45
5	6.34 (6.51)	d	2.4	1	97.62
6	-	-	-	-	147.94
7 (O)	-	-	-	-	-
8	-	-	-	-	148.97
9	6.29 (6.44)	s	-	1	106.07
10	-	-	-	-	142.53
11	-	-	-	-	132.94
12	8.23 (8.80)	dd	7.8	1	125.34
13	7.63 (7.62)	ddd	8.1, 7.5, 1.2	1	131.66
14	7.59 (7.66)	ddd	7.5, 7.5, 1.2	1	131.1
15	8.49 (9.00)	dd	7.5, 0.9	1	125.24
16	-	-	-	-	132.05
17	-	-	-	-	167.11
18 (N)	-	-	-	-	-
19 (N)	-	-	-	-	-
20a	3.43 (3.26)	q	7.2	2	45.96
20b		q		2	
21a	1.20 (1.06)	t	7.2	3	13.08
21b		t		3	
22 (N) a *	(10.53)	s	-	1	-
22 (N) b *	-	-	-	-	-

†Data taken from sample dissolved in pyridine-d_5 are shown in brackets.

Table 3.

Comparison of ^{1}H and ^{13}C chemical shift data acquired for NB and RNB in methanol-d_4 solutions expressed as the chemical shift difference, $\Delta\delta_a = \delta_a^{NB} - \delta_a^{RNB}$ where δ_a represents the chemical shift at position 'a' in the molecule. Numbers in bold refer to $|\Delta\delta_a^{H}| \geq 0.5$ ppm and $|\Delta\delta_a^{C}| \geq 7.0$ ppm; numbers in *italic* refer to resonances showing the smallest chemical shift changes.

Position	Δδ ^{1}H (ppm)	Δδ ^{13}C (ppm)
1	-	4.05
2	0.45	2.83
3	**0.67**	6.56
4	-	6.06
5	**0.53**	-0.46
6	-	1.83
7 (O)	-	-
8	-	4.21
9	**0.53**	**-8.25**
10	-	**-7.31**
11	-	**-8.69**
12	*0.04*	*0.43*
13	0.17	-0.67
14	0.33	2.59
15	0.36	*-0.38*
16	-	1.38
17	-	-4.03
18 (N)	-	-
19 (N)	-	-
20a	0.26	1.2
20b	-	-
21a	*0.14*	*-0.01*
21b	-	-
22 (N) a*	**-0.65**[†]	-
22 (N) b*	-	-

[†] Comparison between DMSO-d_6 (NB) and pyridine-d_5 (RNB) solvents

Table 4.

Calculated parameters for TH self-assembly in D_2O at T = 298 K, pD=7.4

Proton	**H1**	**H2**	**H3**
δ_m, ppm	7.909	7.260	7.149
δ_d, ppm	7.429	6.918	6.680
$\Delta\delta$, ppm	0.480	0.342	0.469
K_{agg}, M^{-1}		430 ± 30	
ΔH_{agg}, $kJmol^{-1}$		–(31 ± 4)	
ΔS_{agg}, $Jmol^{-1}K^{-1}$		–(54 ± 6)	

Table 5.

Calculated parameters for NB in aqueous phosphate buffer at T = 298 K.

Proton	**H2**	**H3**	**H5**	**H9**	**H13**	**H15**
δ_m, ppm	8.185	7.484	7.075	7.119	7.971	9.173
δ_d, ppm	7.262	6.874	6.320	6.284	7.448	8.138
$\Delta\delta$, ppm	0.923	0.610	0.755	0.835	0.523	1.035
K_{agg}, M^{-1}	5600 ± 1100					
ΔH_{agg}, kJ mol^{-1}	- (31 ± 2)					
ΔS_{agg}, J mol^{-1} K^{-1}	- (34 ± 7)					

Table 6.

Summary of diffusion coefficients determined by NMR at 298 K for different concentrations of TH in aqueous and methanol solutions and for NB in aqueous solution.

	TH	**NB**
	D / m^2 s^{-1} × 10^{10}	
Aqueous Solution	**4**	**1**
x_0 = 5 mM	3.944	1.673
x_0 = 0.2 mM	5.730	3.994
Methanol Solution	**5**	
x_0 = 5 mM	8.45	-
x_0 = 2 mM	13.94	-
x_0 = 0.2 mM	20.0	-

Figure Captions

Figure 1. a) UV-vis spectra of NB solution (10^{-4} M) in water (thin solid line), in 0.1 M aqueous NaOH (thick dashed line), in pyridine (thin dashed line) and a toluene extract from 10^{-4} M aqueous NaOH solution (thick line). **b)** [INSET] NB (10^{-3} M) in a 0.1 M NaOH/toluene bi-phasic system together with NMR sample tube containing NB solubilized in pyridine-d_5 (the solution coats the inside of the NMR tube above the bulk sample in order to show the true colour of the solution).

Figure 2. Aromatic resonance region of a) the 600 MHz 1D ^{1}H NMR spectrum of NB in DMSO-d_6 [Inset in methanol-d_4] and b) the 150 MHz 1D ^{13}C-{^{1}H} NMR spectrum of NB in methanol-d_4 showing in each case the final designation of resonance assignments. In a) sample impurities (10%) appear as lower intensity NMR signals. In b) a transmitter glitch is observed in the region of 102 ppm.

Figure 3. Aromatic resonance region of a) the 600 MHz 1D ^{1}H NMR spectrum of RNB and b) the 150 MHz 1D ^{13}C-{^{1}H} NMR spectrum of RNB in methanol-d_4 showing in each case the final designation of resonance assignments. In a) sample impurities (10%) appear as lower intensity NMR signals. In b) a transmitter glitch is observed in the region of 102 ppm.

Figure 4. Aromatic resonance cross-peak region of the 600 MHz 2D [^{1}H, ^{1}H] DQFCOSY NMR spectrum of NB in DMSO-d_6 with correlations identified according to assignments.

Figure 5. Aromatic to aromatic cross-peak region of the 600 MHz 200 ms 2D [^{1}H, ^{1}H] NOESY NMR spectrum of NB in DMSO-d_6. Key intra-molecular correlations used to establish the correct assignment of resonances for protons associated with ring **A** are shown annotated in **bold**. Intermolecular correlations associated with the self-assembly of the molecule are also shown as ***bold italicized*** annotations. The assigned 1D ^{1}H NMR spectrum of NB is shown as a projection above the 2D NOESY NMR data.

Figure 6. Overlays of the aromatic cross-peak region in 2D [^{1}H, ^{13}C] HSQC (black) and HMBC (red) NMR data acquired at a field strength of 14.1 T for a) NB and b) RNB in methanol-d_4. Annotation is shown for cross-peaks arising from $^{1}J_{HC}$ (black) and $^{n>1}J_{CH}$ (red) together with labelling of the projection spectra.

Figure 7. 600 MHz 1D ^{1}H NMR spectrum (**a**) and 1000 ms 2D [^{1}H, ^{1}H] NOESY NMR spectrum (**b**) of RNB in pyridine-d_5. Assignments of key resonances are shown at the top of the figure. The NH signal at δ^{1}H = 10.53 ppm integrates to one proton equivalent and shows a strong NOE to H9 as indicated. The NOE to H15 arises through spin-diffusion effects at the longer mixing time and is not apparent at the shorter mixing time of 270 ms (data not shown). Ridges due to t_1 noise arise from the presence of residual solvent resonances, the latter being removed by a multi signal solvent suppression routine (see experimental section for details).

Figure 8. Temperature and concentration dependence of ^{1}H chemical shifts [H1 (◆), H2 (■) and H3 (●)] for TH in ionic and neutral forms. **a)** Temperature dependence (278 K – 353 K) of ^{1}H chemical shifts at concentrations of 2 mM (solid line, solid symbols) and 0.2 mM (dashed line, open symbols) in buffered aqueous solution. **b)** As for (**a**) but in methanol-d_4 with NaOD over the temperature range 278 K – 318 K. **c**) Concentration dependence of TH ^{1}H chemical shifts under buffered aqueous solution conditions. **d)** As for **c**) in methanol-d_4 with NaOD. Concentration dependencies were measured at a sample temperature of 298 K.

Figure 9. Model of the self-assembly dimer unit of NB in DMSO-d_6 as suggested by NOE data. Key NOEs are indicated by black double-headed arrows: Left/Front NOE measured between protons H15 and H2**;** Right/Rear NOE measured between protons H9 and H5. Relative orientation of molecule planes is shown by the smaller inset figure.

Figure 10. Evolution of ^{1}H NMR chemical shifts of the aromatic proton resonances of NB **a)** with temperature for x_0 = 2 mM in aqueous phosphate buffer and **b)** with concentration at T = 298 K.

Figure 1

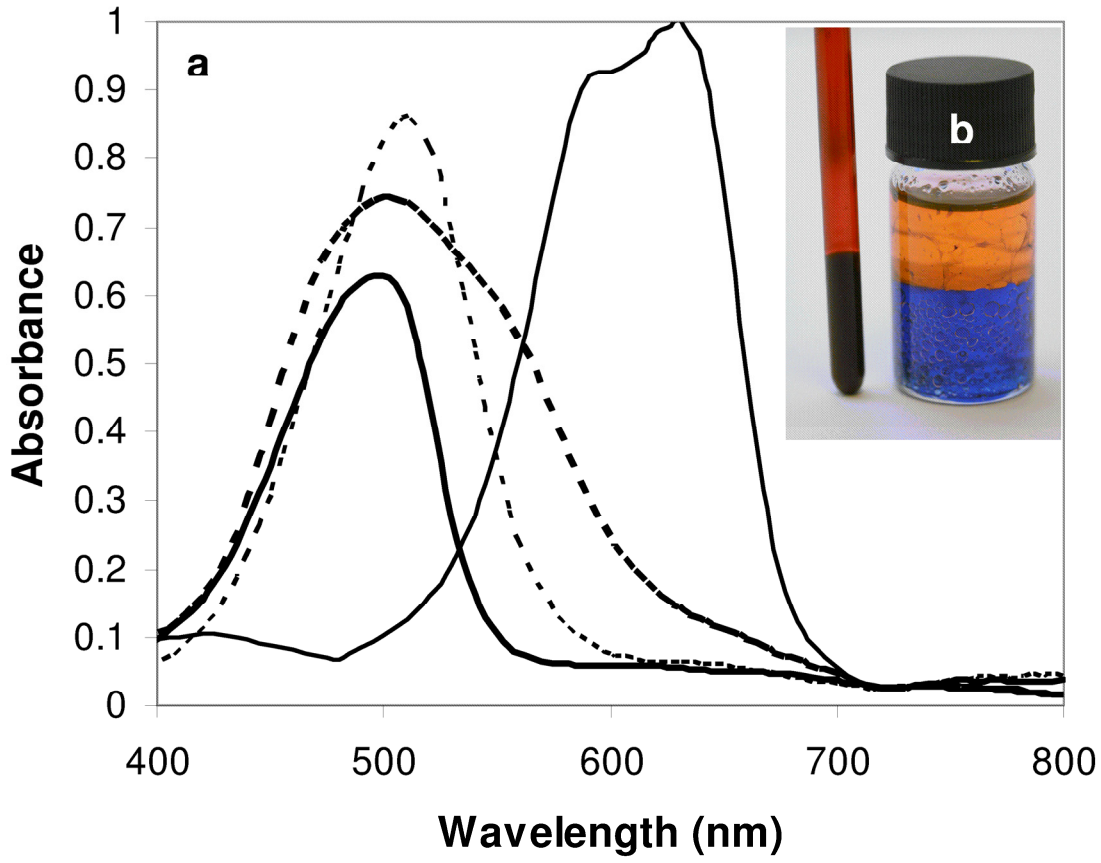
a
b
Absorbance
Wavelength (nm)
0
0.1
0.2
0.3
0.4
0.5
0.6
0.7
0.8
0.9
1
400
500
600
700
800

Figure 2

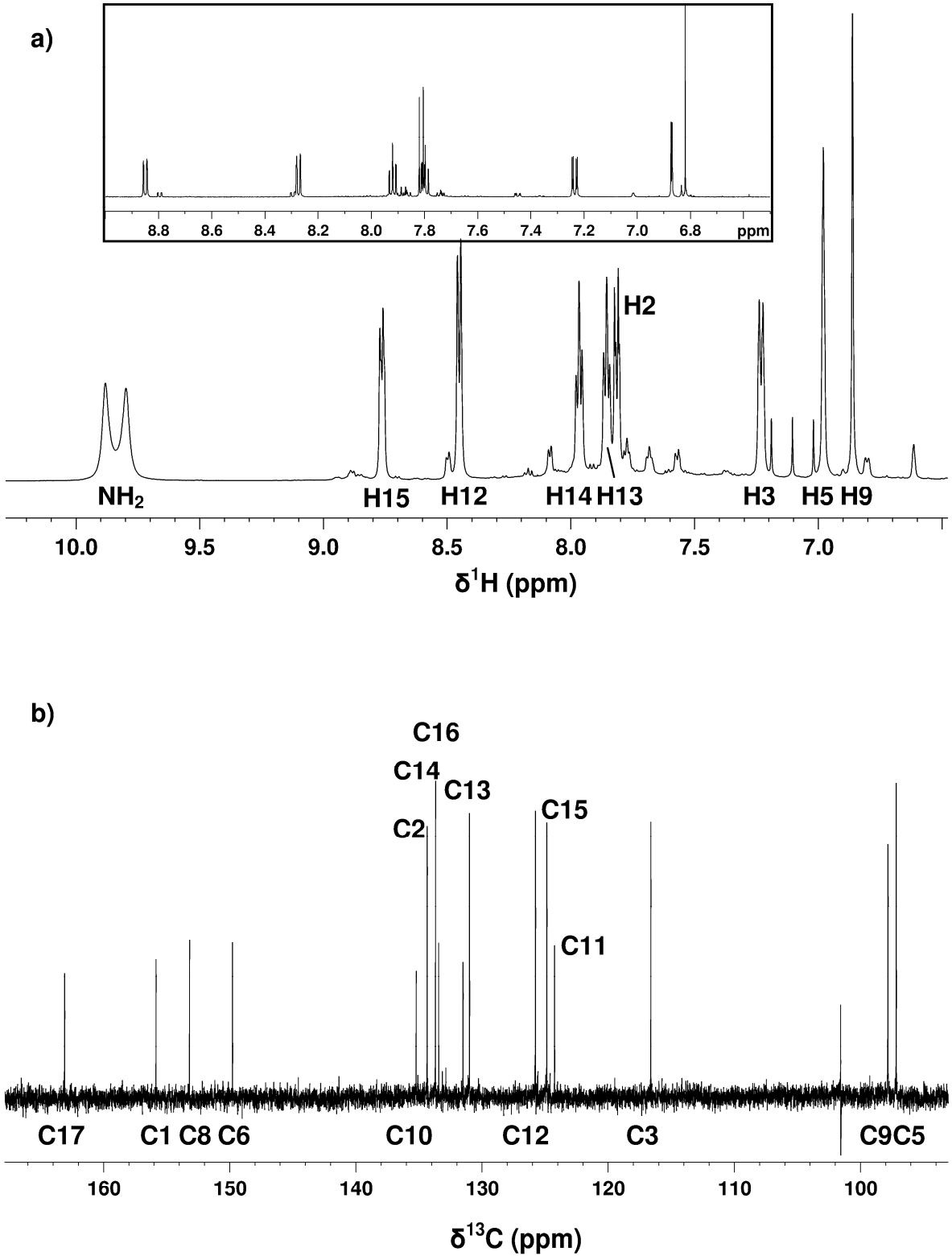
a)
8.8
8.6
8.4
8.2
8.0
7.8
7.6
7.4
7.2
7.0
6.8
ppm
H2
NH2
H15
H12
H14
H13
H3
H5
H9
10.0
9.5
9.0
8.5
8.0
7.5
7.0
δ1H (ppm)
b)
C16
C14
C13
C15
C2
C11
C17
C1
C8
C6
C10
C12
C3
C9
C5
160
150
140
130
120
110
100
δ13C (ppm)

Figure 3

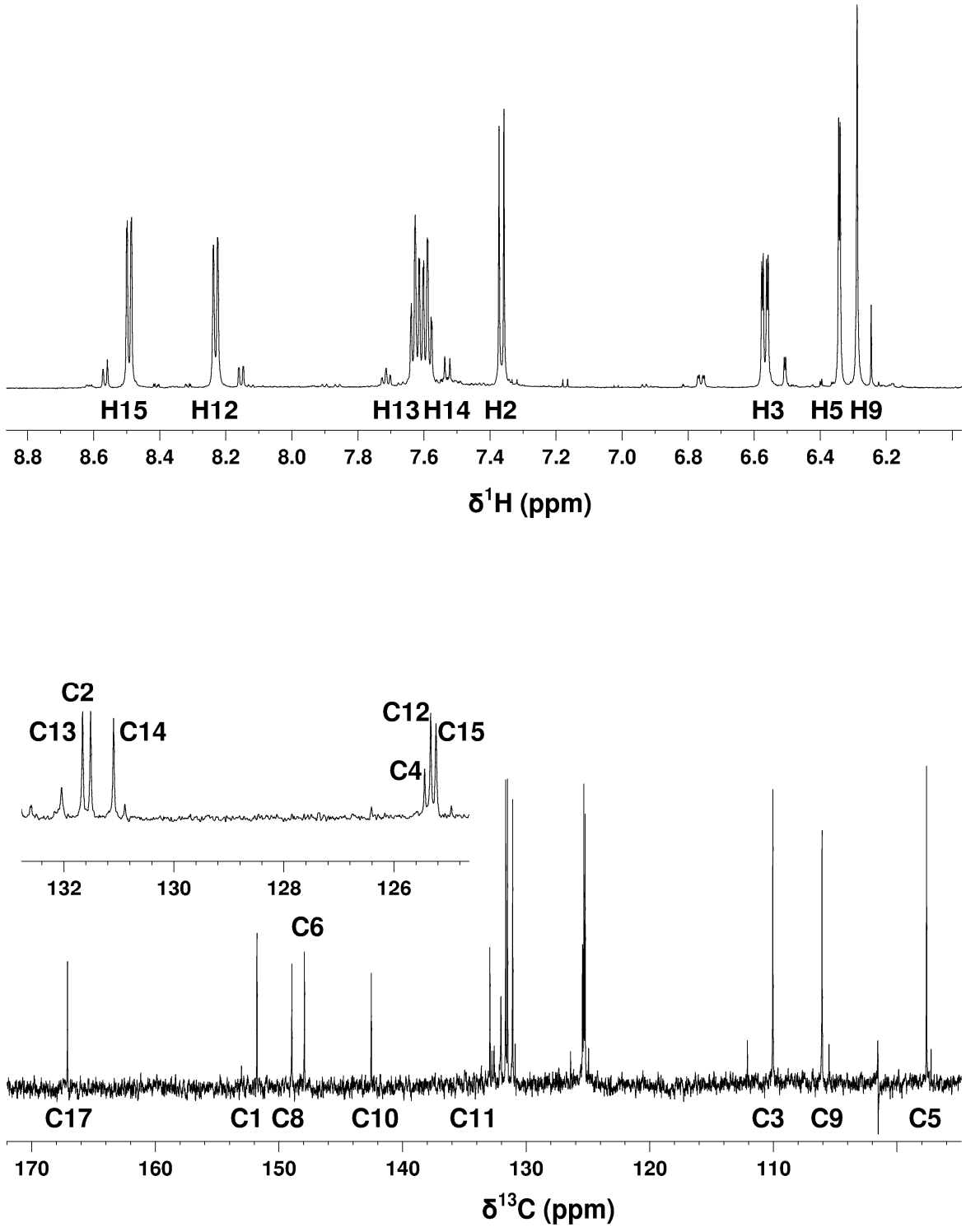
H15
H12
H13
H14
H2
H3
H5
H9
8.8
8.6
8.4
8.2
8.0
7.8
7.6
7.4
7.2
7.0
6.8
6.6
6.4
6.2
δ1H (ppm)
C2
C13
C14
C12
C15
C4
132
130
128
126
C6
C17
C1
C8
C10
C11
C3
C9
C5
170
160
150
140
130
120
110
δ13C (ppm)

Figure 4

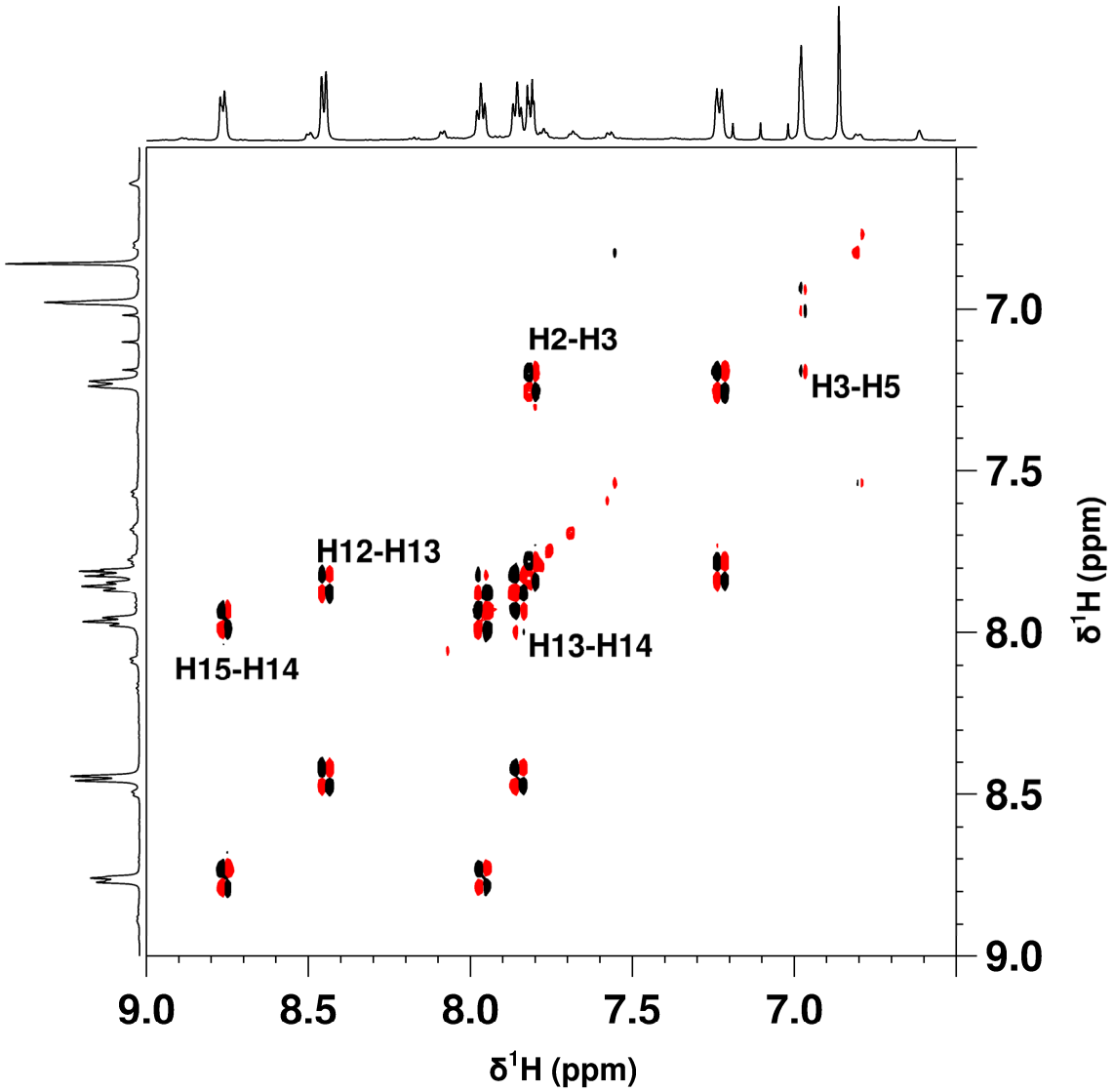
H2-H3
H3-H5
H12-H13
H13-H14
H15-H14
9.0
8.5
8.0
7.5
7.0
δ¹H (ppm)
7.0
7.5
8.0
8.5
9.0
δ¹H (ppm)

Figure 5

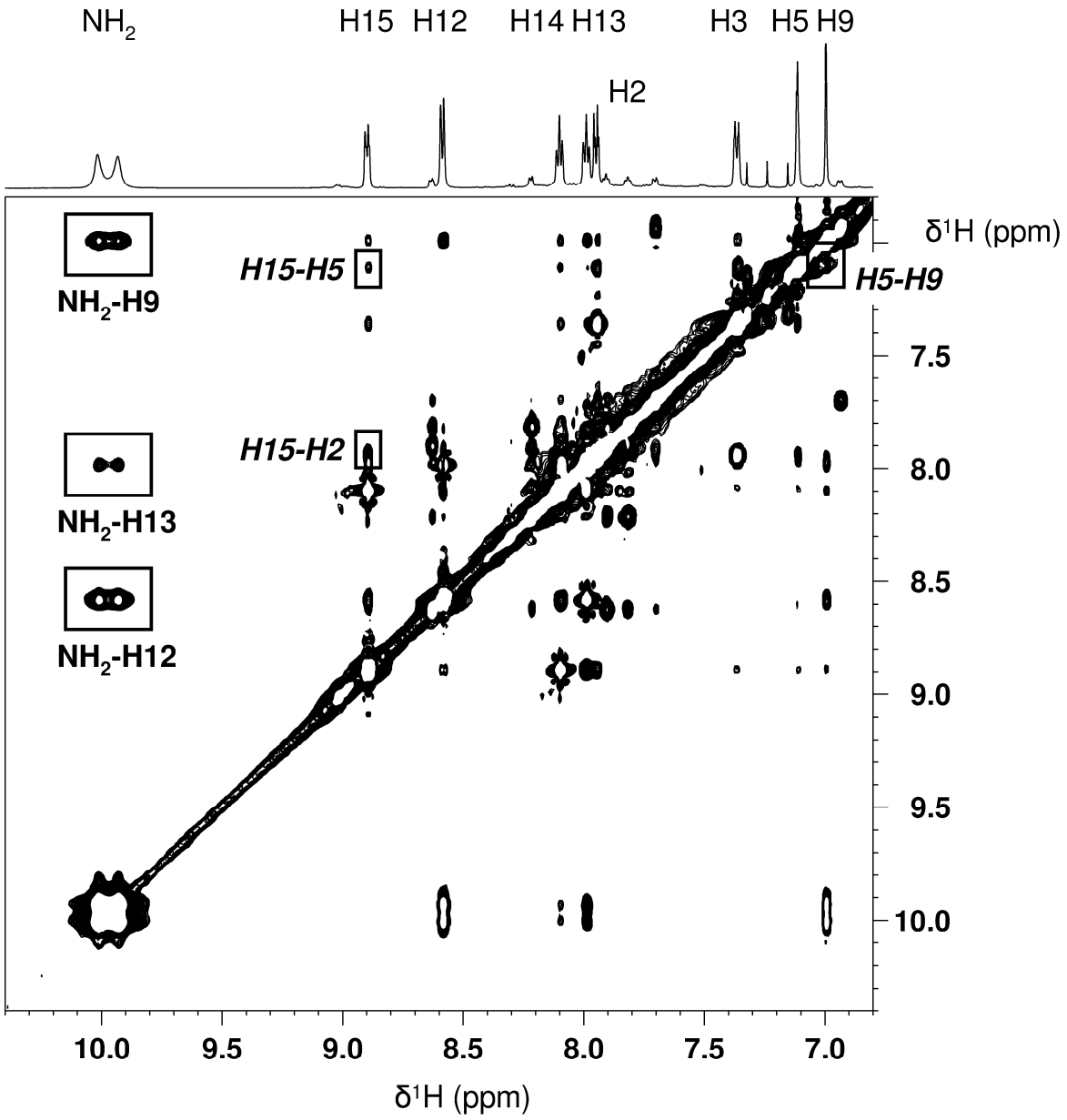
NH2
H15
H12
H14
H13
H2
H3
H5
H9
δ1H (ppm)
H15-H5
H5-H9
H15-H2
NH2-H9
NH2-H13
NH2-H12
7.5
8.0
8.5
9.0
9.5
10.0
10.0
9.5
9.0
8.5
8.0
7.5
7.0
δ1H (ppm)

Figure 6

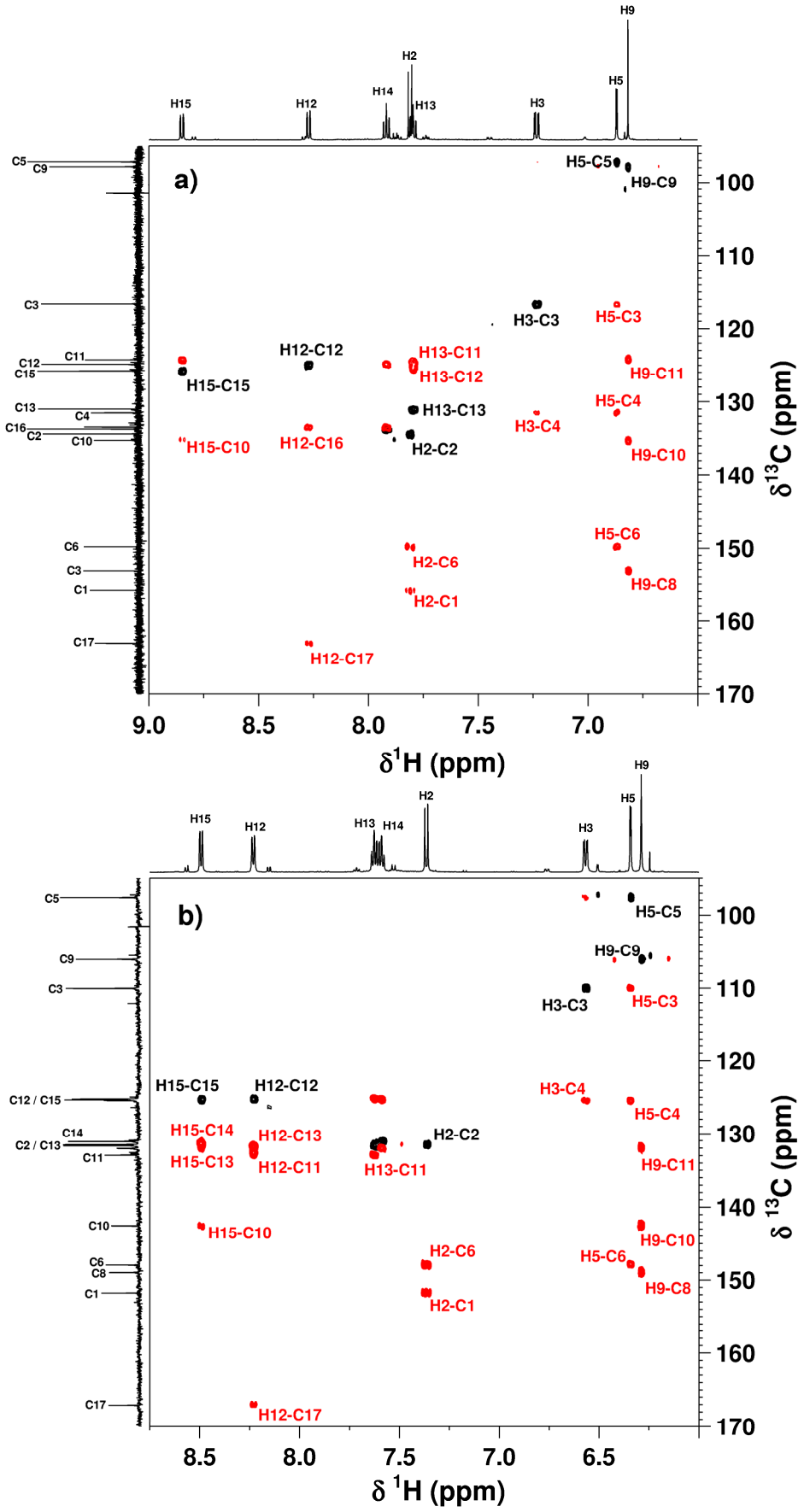
a)
H15
H12
H14
H2
H13
H3
H5
H9
H5-C5
H9-C9
H3-C3
H5-C3
H12-C12
H13-C11
H13-C12
H9-C11
H15-C15
H5-C4
H13-C13
H3-C4
H2-C2
H9-C10
H15-C10
H12-C16
H5-C6
H2-C6
H9-C8
H2-C1
H12-C17
C5
C9
C3
C12
C11
C15
C13
C4
C16
C2
C10
C6
C3
C1
C17
100
110
120
130
140
150
160
170
9.0
8.5
8.0
7.5
7.0
δ1H (ppm)
δ13C (ppm)
b)
H15
H12
H13
H14
H2
H3
H5
H9
H5-C5
H9-C9
H3-C3
H5-C3
H15-C15
H12-C12
H3-C4
H5-C4
H15-C14
H12-C13
H2-C2
H15-C13
H12-C11
H13-C11
H9-C11
H15-C10
H9-C10
H2-C6
H5-C6
H9-C8
H2-C1
H12-C17
C5
C9
C3
C12 / C15
C14
C2 / C13
C11
C10
C6
C8
C1
C17
100
110
120
130
140
150
160
170
8.5
8.0
7.5
7.0
6.5
δ 1H (ppm)
δ 13C (ppm)

Figure 7

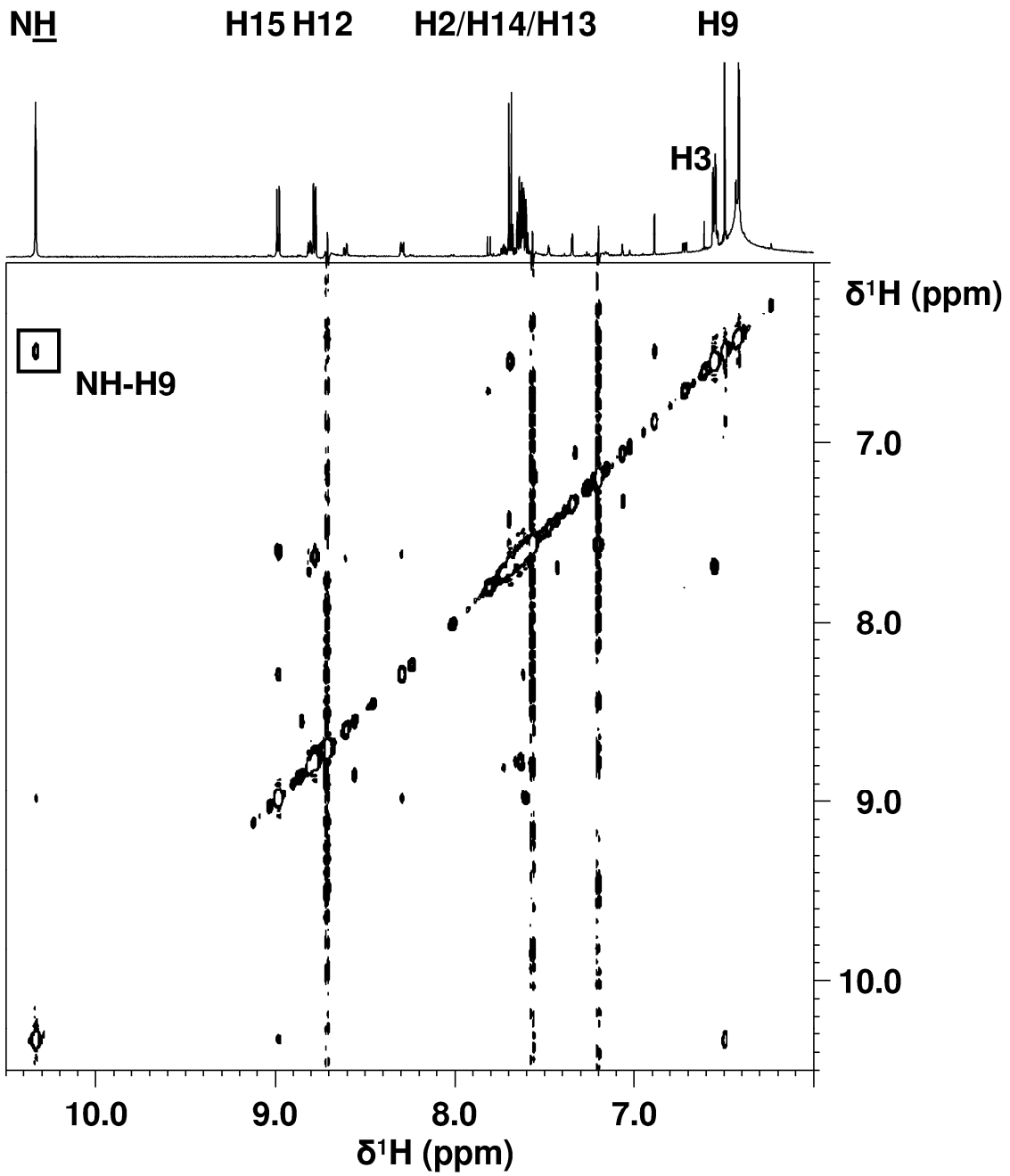
NH
H15 H12
H2/H14/H13
H9
H3
NH-H9
δ¹H (ppm)
7.0
8.0
9.0
10.0
10.0
9.0
8.0
7.0
δ¹H (ppm)

Figure 8

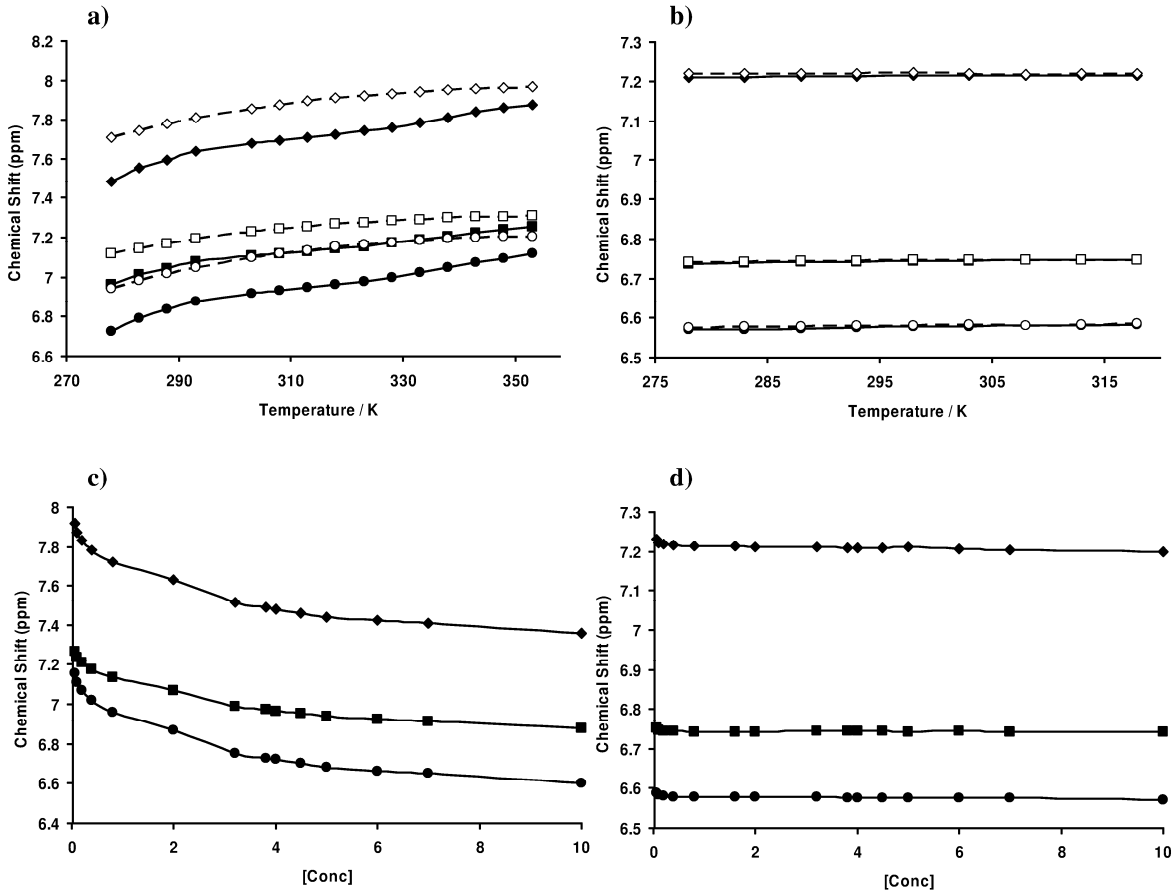
a)
Chemical Shift (ppm)
Temperature / K
b)
Chemical Shift (ppm)
Temperature / K
c)
Chemical Shift (ppm)
[Conc]
d)
Chemical Shift (ppm)
[Conc]

Figure 9

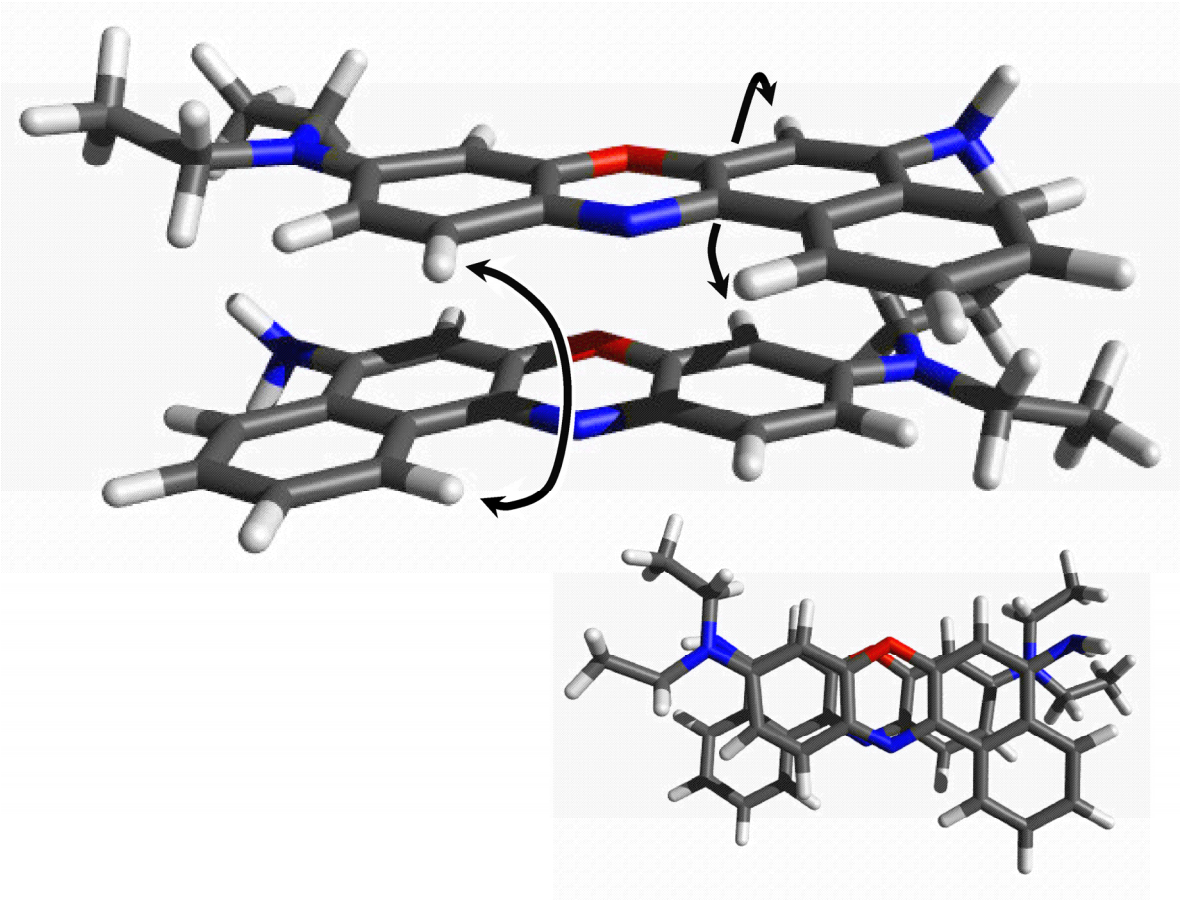

Figure 10

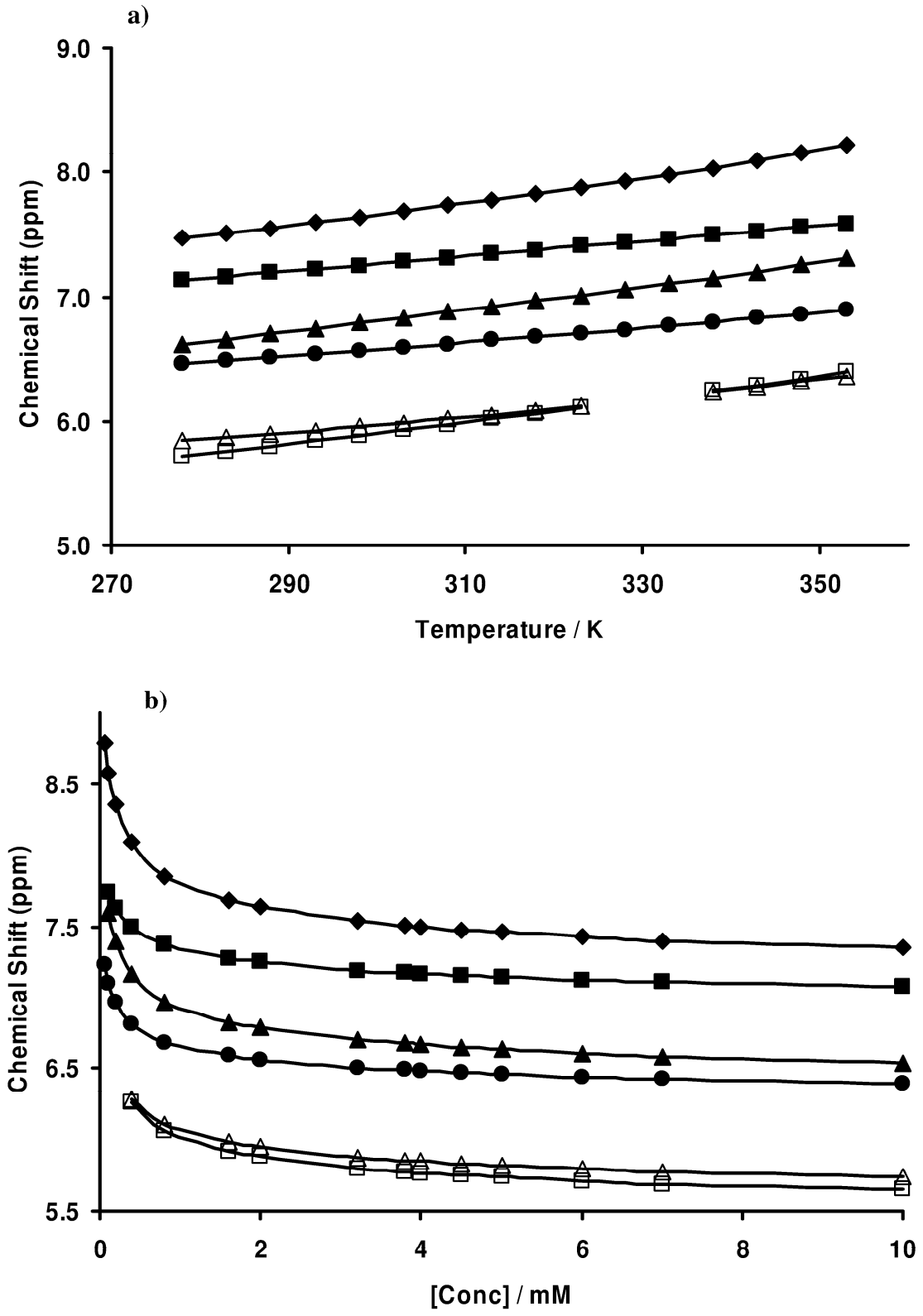
a)
9.0
8.0
7.0
6.0
5.0
Chemical Shift (ppm)
270
290
310
330
350
Temperature / K
b)
8.5
7.5
6.5
5.5
Chemical Shift (ppm)
0
2
4
6
8
10
[Conc] / mM